Electrochemical Response of Aluminum and Al Alloy Anodes in Seawater for Cathodic Protection: A Finite Element Method Study

M'hamed Ouadah[1, 2] and Abderrahmane Younes[3,*]

[1]*National Higher School of Advanced Technologies, Bab El Oued, Alger, Algeria*
[2]*Polytechnic National Higher School, El Harrach, Algiers, Algeria*
[3]*Research Centre in Industrial Technologies (CRTI), Cheraga, Algiers, Algeria*
[*]Corresponding author: younesabdo11@gmail.com

Received 22/04/2024; accepted 10/10/2024
https://doi.org/10.4152/pea.2026440305

Abstract
This study investigated the electrochemical performance of pure Al and Al alloy anodes in Sw environments for CP real-world applications, such as marine environments, under various operational conditions. Experimental results showed a significant activation of Al alloy anodes compared to pure Al, as indicated by a more anodic shift in OCP and a marked increase in j_{corr}. The impact of varying DAC and changes in Sw conductivity on CP performance was also herein explored. These factors notably influenced both E_{corr} and j from CP, resulting in deviations from expected design values.

Keywords: Al alloy; CP analysis; electrochemical calculations; modeling investigations; Sw.

Introduction•

The exploration of electrochemical behaviors in Al alloys has been primarily driven by their application in batteries and as anode materials in CP systems [1, 2]. Al is the ideal choice for crafting galvanic SA to thwart the corrosion of steel structures, due to its low electrode E, high current capacity, low density and cost-effectiveness [3, 4]. However, contrary to SA requirements, Al corrosion tends to manifest through pitting rather than being uniform, due to immediate formation of a passive oxide layer upon exposure to the environment [5, 6].

Numerous studies have explored the activation of electrochemical anodes [7-10]. Ce addition to SA from Al–Zn–In in a NaCl solution, to enhance their electrochemical properties and corrosion resistance, was performed by [11], and it was found to increase current efficiency, improving the anodes efficiency. Furthermore, Ce promotes a uniform surface corrosion, contributing to longer-lasting anode performance.

In their review, [12] have highlighted the potential of Na^- batteries as a promising alternative to Li+ batteries, with a focus on developing high-performance carbon

• The abbreviations list is in pages 230-231.

anodes and providing a comprehensive guide to electrochemical and physicochemical evaluation techniques.

Advancements in metalloid anodes (Si, Ge and B) for air batteries, were reviewed by [13], highlighting their potential to surpass traditional metal-air batteries. Si and Ge anodes have demonstrated high energy density, longer discharge times and environmental benefits, while B and Si have shown promising electrochemical performance. The article has also explored metalloid composites and computational studies, paving the way for future innovations in air battery technologies.

Key scientific challenges in the development of Zn^- batteries, as a safer and more affordable alternative to Li+ batteries, particularly for stationary energy storage, have been reviewed [14]. Their article addresses issues such as Zn^{2+}/proton co-intercalation, limitations of conversion chemistry, desolvation penalties, Zn dendrite growth and cathode material optimization.

Several researches have also proposed solutions and valuable insights for overcoming these obstacles to advance Zn^- technology. For instance, [15] has scrutinized the performance of SA from Al–Zn–In–Mg–Ti in a simulated deep water environment, employing various techniques. They have observed an accelerated corrosion process, primarily due to the heightened cathodic process, leading to a significant drop in efficiency in deep water conditions.

In a laboratory study conducted by [16], in natural Sw, A1–Zn–In anode has displayed an anode capacity approximately 7–10% lower and E that was 5-20 mV higher at 50 than at 1 Atm.

The present work has compared electrochemical dissolution processes of pure Al and Al alloys as anodes for CP of steel structures in a Sw medium. Electrochemical characteristics of these anodes were examined in an artificial Sw electrolyte through OCP, PDP and EIS measurements. Microstructures of the anodes, pre- and post-measurements, were analyzed via optical microscopy. To assess the efficiency of Al alloy anode under various exploitation conditions, such as varying Sw conductivity and different DAC, a SA model was simulated using FEM. The polarization curves of Al alloy anode and steel cathode in simulated Sw served as boundary conditions in the simulation model.

Materials and methods

Microstructure analysis

In this study, the National Naval Repair Company, a reputable ship repair company based in Algeria, has meticulously crafted an Al alloy anode. The fabrication process and the alloy composition of Al alloy sample are illustrated and summarized in Fig. 1 and Table 1, respectively. Notably, the pure Al sample exhibited a remarkable purity level of 99.95%.

To analyse the microstructures of the specimens, optical microscopy was employed. The specimens underwent a meticulous preparation process, including successive grinding to 2000 grit, using SiC paper, fine polishing with a 0.3 μm Al dispersion, and etching with a solution made of 2.5% HNO_3, 1.5% HCl and 1% HF. This comprehensive approach ensured a detailed and accurate examination of Al alloy's microstructural features.

Figure 1: Pure Al alloy.

Table 1: Composition breakdown of Al alloy.

Al	Zn	Fe	Mg	Cu	Ni
93.292	5.839	0.593	0.047	0.021	0.001
Sb	**Sn**	**Ti**	**Cr**	**Mn**	**Si**
028	0.082	0.003	0.001	0.005	0.079

Electrochemical measurements

Electrochemical measurements were conducted using a Bio-Logic SP-150 electrochemical workstation, interfaced with a PC, for precise control. A three-electrode system was employed, wherein pure Al and Al alloy specimens served as working electrodes, with a geometric exposed area of 1 cm². Prior to each experiment, the electrodes underwent successive polishing with emery paper of increasing fineness (up to 500, 1200, 2000 and 4000 grade), followed by fine polishing with a 0.3 µm grit alumina suspension. Subsequently, the electrodes were degreased with acetone and thoroughly rinsed with distilled water. A SCE functioned as reference electrode, while a Pt wire served as counter electrode. All electrochemical experiments were conducted at room temperature, with the solution gently stirred using a magnetic stirrer. E values presented in this article are referenced to SCE scale. The electrolyte used in the cell was meticulously prepared following ASTM D 1141-90. Comprehensive details regarding experimental conditions and chemical composition of primary salts in the electrolyte solution are provided in Tables 2 and 3, respectively.

Table 2: Composition of mineral salts in an artificial Sw solution.

Salt	NaCl	$MgCl_2$	Na_2SO_4	$CaCl_2$	KCl	$NaHCO_3$
Amount ($g.L^{-1}$)	24.53	5.20	4.09	1.16	0.69	0.201

Table 3: Experimental conditions and physicochemical characteristics of artificial Sw.

Salinity (g/L^{-1})	Conductivity (mS/cm^{-1})	pH	T (°C)
35	21.6	6.5	20.6

Distilled water, sourced for its purity, was employed throughout the experiments, and all solutions were meticulously prepared using analytical-grade chemicals. OCP was continuously monitored for 900 sec. in the electrolyte solution. To gain deeper insights into electrochemical and physico-chemical phenomena associated with electrode reactions, EIS studies were conducted. Spectra were recorded in a frequency range from 100 kHz to 10 mHz, using a 5 mV peak-to-peak signal

amplitude. PDP curves were acquired by scanning within a range of ±500 mV/OCP, employing a scan rate of 1 mV/s, from the cathodic to anodic direction. The determination of j_{corr} was achieved through extrapolation of anodic and cathodic Tafel lines at E_{corr}. These comprehensive methodologies were employed to thoroughly unveil electrochemical processes and associated phenomena.

CP simulation

Herein, fundamental components of CP system encompassed a sacrificial Al alloy anode (Γ_1), a steel cathode (Γ_2) and Sw (**Ω**). The design of CP systems requires solving Laplace's equation, $\nabla^2\phi = 0$, while considering relevant boundary conditions to determine E distribution and j within the solution. Boundary conditions are depicted in Fig. 2.

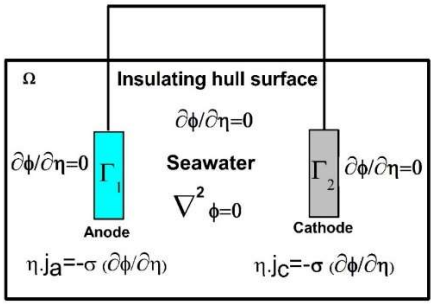

Figure 2: Schematic representation of boundary conditions in CP system, where Γ_1 and Γ_2 represent the anode and cathode, respectively.

Distinct boundary conditions were applied based on their nature. For symmetry boundaries, the following condition was employed [13-17]:

$$\frac{\partial \emptyset}{\partial n} = n.\nabla\emptyset = 0 \qquad (1)$$

Prescribed boundary conditions for anode and cathode surfaces were:

$$n.J_a = -\sigma\frac{\partial \emptyset}{\partial n} = f_a(\emptyset) \qquad (2)$$

$$n.J_c = -\sigma\frac{\partial \emptyset}{\partial n} = f_c(\emptyset) \qquad (3)$$

where ϕ is E, J_a and J_c denote j at the anode and cathode, respectively, σ is electrolyte conductivity and n is normal boundary surface. Functions $f_a(\phi)$ and $f_c(\phi)$ represent the connection between j and E at the anode and cathode, respectively. The expression for j at the electrode surface can be formulated in terms of Butler-Volmer relation.

$$J = J_0\left(e^{\frac{\alpha_{aF}\eta}{RT}} - e^{\frac{\alpha_{bF}\eta}{RT}}\right) \qquad (4)$$

where J_0 is exchange j, R is universal gas constant, T is the electrode absolute temperature, F is Faraday's constant, η is over potential,α_b and α_a are cathodic and anodic charge transfer coefficients, respectively.

Results and discussion

Microstructure

Fig. 3 illustrates the microstructure of both pure Al and Al alloy. Both anodes exhibit a consistent and homogeneous grain size, with a regular distribution across the entire surface. However, there is a notable distinction in aspect between the two.

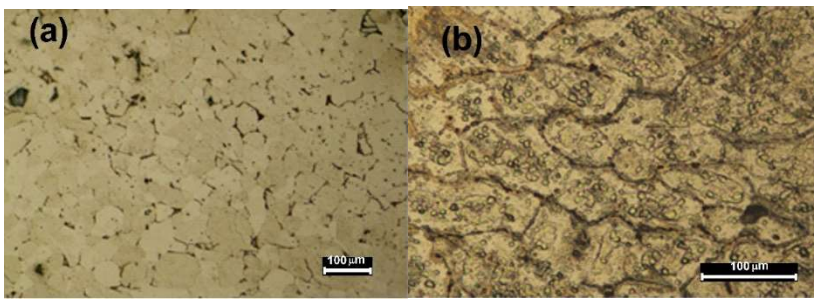

Figure 3: Optical micrographs depicting **(a)** pure Al and **(b)** Al alloy microstructures.

OCP evolution

Temporal evolution of OCP, concerning the studied materials immersed in artificial Sw, for 900 s, is depicted in Fig. 4.

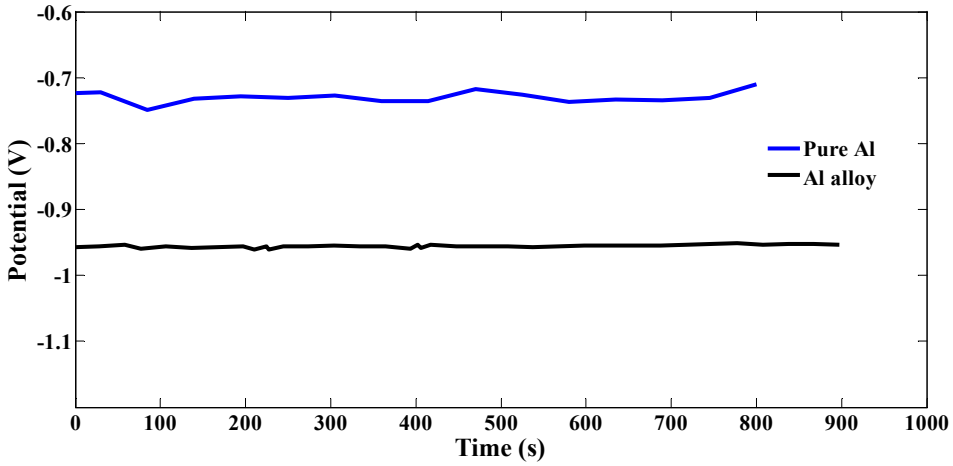

Figure 4: Temporal changes in OCP for pure Al and Al alloy materials in a Sw solution.

Pure Al exhibited a relatively mild shift of approximately 5 mV towards more anodic E, before stabilization. In contrast, Al alloy displayed a rapid and pronounced shift towards the cathodic direction, within initial seconds of immersion, reaching a steady state after 300 sec. These variations can be ascribed to gradual changes in Al oxide layer forming promptly on the pure Al surface and to Al alloy ongoing dissolution in the electrolyte solution.

PDP

Fig. 5 illustrates PDP curves of Al alloy and pure Al anodes immersed in a Sw solution. Notably, no passivation was seen on the anodic part of Al alloy plot. However, variations on the cathodic side were evident, attributed to an apparent

catalytic effect of surface elements on O_2 reduction. E_{corr} value of Al alloy notably shifted to more negative values, accompanied by a significantly higher j compared to pure Al. This discrepancy implies that the alloyed anode was more prone to corrosion in Sw solution than the pure anode.

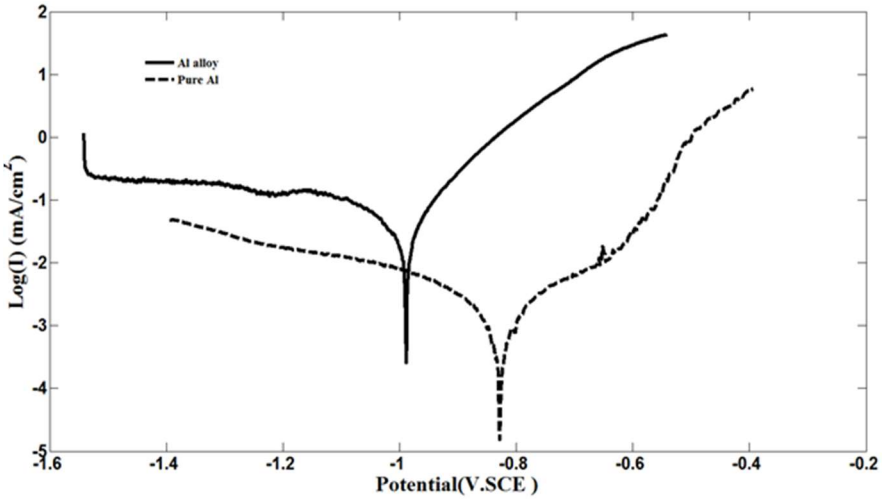

Figure 5: PDP curves for pure Al and Al alloy materials in a Sw solution.

On the anodic part of Al alloy curve, a distinct active-passive transition was seen, a phenomenon not observed for pure Al. This distinction arose from the immediate formation of a passive film on the Al surface, which could be enhanced by the addition of alloying elements that originate precipitates, amplifying Al action. Electrochemical parameters from PDP are summarized in Table 4.

Table 4: Electrochemical parameters derived from PDP curves.

Samples	E_{ocp} (mV)	E_{corr} (mV)	I_{corr} ($\mu A/cm^{-2}$)
Pure Al	-786	-828	2.6
Al alloy	-962	-990.6	49.4

The performance of pure Al and Al alloy anodes was evaluated and compared with previously reported data by [18], who have demonstrated that microstructural evolution plays a crucial role in enhancing their performance regarding electrochemical activity, corrosion resistance and structural integrity, which are linked to grain refinement and uniform consumption of grain boundaries.

Corrosion mechanism

Polarization measurements offer mechanistic insights into anodic reactions. The following mechanisms are postulated for anodic and cathodic reactions of Al corrosion processes in a Sw solution. Anodic reaction involved Al dissolution and cathodic reaction pertains to dissolved oxygen reduction, as expressed by Eqs. (5) and (6) [19]:

$$4Al \rightarrow 4Al^{3+} + 12e^{-} \qquad (5)$$

$$3O_2 + 6H_2O + 12e^- \rightarrow 12OH^- \quad (6)$$

In instances where the predominant cathodic reaction involves oxygen reduction, the corrosion process generates an oxygen concentration gradient from the bulk electrolyte to the corroding surface. This gradient results from oxygen consumption at the solid-solution interface, highlighting the significant role played by its diffusion in corrosion processes. Al hydroxide formation is described by Eq. (7):

$$4Al + 3O_2 + 6H_2O \rightarrow 4Al(OH)_3 \quad (7)$$

Subsequently, Al oxide is generated on the electrode surface through Al hydroxide transformation, as expressed by Eq. (8):

$$2Al(OH)_3 \rightarrow Al_2O_3 + 3H_2O \quad (8)$$

The formed oxide film does not provide adequate protection against attacks from chloride anions. Due to their diminutive size, chloride ions can easily permeate the passive film and reach the bulk substrate, leading to the dissolution of Al when exposed to a Sw solution.

Fig. 6 depicts the characteristic pit morphology observed on the corroded surfaces of pure Al and Al alloy following PDP measurements. Al alloy surface reveals a multitude of hemispherical pits that are notably larger and deeper than those formed on pure Al. In the case of Al alloy, the initiation of matrix dissolution occurs at active sites through pitting. Subsequently, flaws on the alloy surface contribute to pitting propagation. In this process, the precipitates within the alloy significantly accelerate the propagation of pits, thus contributing to the activation of the alloy [20].

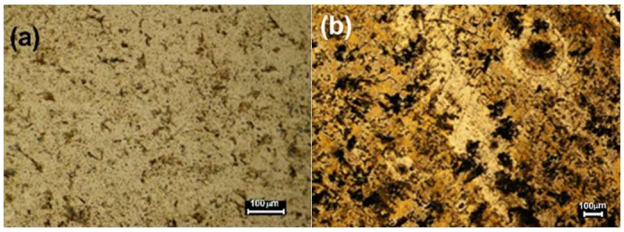

Figure 6: Optical micrographs revealing the morphology of corroded surfaces for **(a)** pure Al and **(b)** Al alloy after PDP in a Sw solution.

Electrochemical impedance diagrams

Fig. 7 displays EIS spectra acquired for both alloyed and pure Al anodes. EIS diagram of Al alloy exhibits a distinctive inductive loop at low frequencies, while no such loop is seen for pure Al anode.

The semicircle in the high-frequency range corresponds to R_{ct}. Notably, R_p value for Al alloy surpassed that of pure Al, agreeing with findings from polarization measurements. This suggests that the inclusion of alloying elements could enhance the anodes' galvanic efficiency. R_p correlated well with the anodes' corrosion rates. To model Al alloy impedance spectra in Sw, the equivalent circuit shown in Fig. 3 was applied.

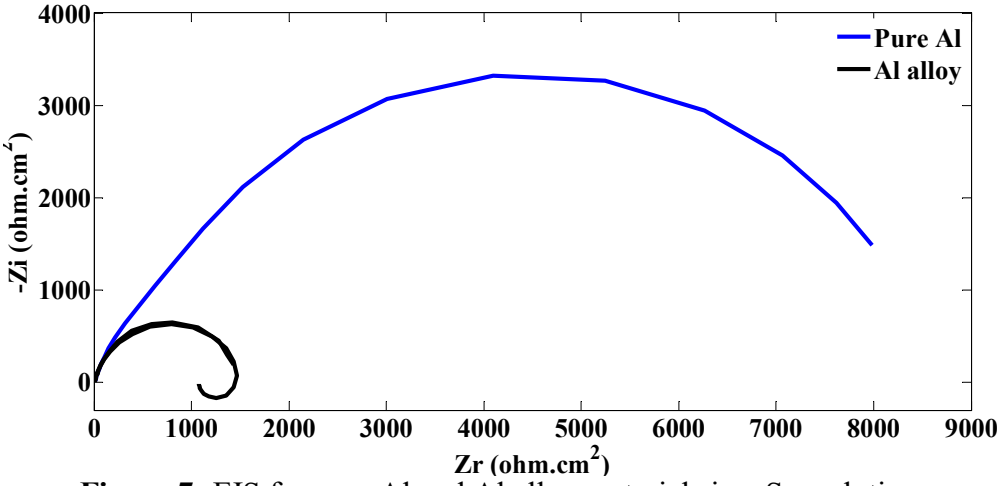

Figure 7: EIS for pure Al and Al alloy materials in a Sw solution.

Table 5 provides optimized fitting parameters and values for Al alloy in Sw, based on the equivalent circuit model presented in Fig. 8.

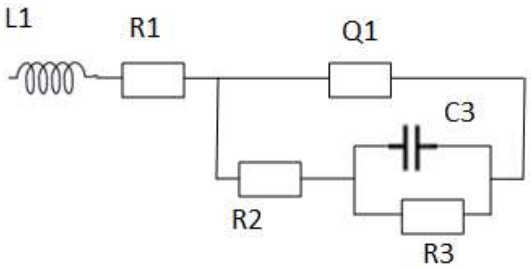

Figure 8: Corresponding equivalent circuits proposed for Al alloy.

Table 5: Fitting parameters and optimum values for Al alloy in Sw using the equivalent circuit model in Fig. 8.

L1	0,1583 10^{-6} H
R1	5,313 Ohm
Q1	30,99 10^{-6} F.$s^{(a-1)}$
A1	0,8608
R2	1 574 Ohm
C3	-0,9851 10^{-3} F
R3	-502,2 Ohm

Several researchers [21, 22] have reviewed the performance of Al alloys as SA in Sw, emphasizing their electrochemical properties and alloy compositions within marine CP systems. The review has concluded that Al alloys, especially those alloyed with zinc and In, outperform pure Al by resisting passivation and offering stable, long-term protection. Although, it was also noted that Sw composition and environmental factors influence anode performance, overall, Al alloys remain a dependable choice for CP in marine environments.

Al anodes electrochemical behaviour in Sw has been investigated by [23], particularly examining the impact of Zn and In as alloying elements. Their research has concluded that these additions markedly improved Al's performance as a SA.

The alloyed anodes demonstrated stable and uniform dissolution and provided consistent corrosion protection by resisting passivation and sustaining high anodic efficiency over time, thereby enhancing their effectiveness for CP in Sw. Electrochemical behaviour of pure Al in the presence of Ga ions or in direct contact with this element has been studied by [24] in chloride, acetic acid solutions and distilled water. Al's enhanced activity was observed in two active regions: one at approximately -1.5 V, where a Ga–Al amalgam was formed after a critical concentration of liquid was reached, resulting in uniform attack due to exothermic Al ion hydrolysis; and another near -1.1 V, especially in chloride media, where solid Ga at the interface facilitated chloride adsorption, leading to depolarization of the anodic reaction and localized attack. Two distinct activation mechanisms have been proposed for each region.

Sacrificial Al alloy CP

The model geometry represents a three-dimensional rectangular electrolyte volume with dimensions of 30 x 30 x 6 cm, featuring an anode (1 x 1 x 0.5 cm) and a cathode (20 x 20 x 0.2 cm), as depicted in Fig. 9. DAC was 0.1 cm. Fig. 10 illustrates PDP curves measured for the steel cathode.

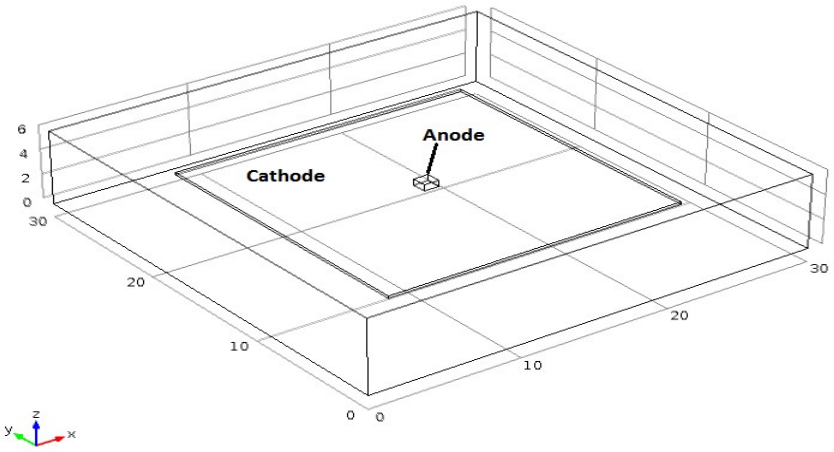

Figure 9: Three-dimensional model geometry featuring Al alloy anode and steel cathode.

Obtained PDP curves from electrochemical measurements of Al alloy anode (Fig. 5) and steel cathode (Fig. 10) in simulated Sw were employed as boundary conditions in the simulation model.

The studies undertaken by [25] on Al-Zn-In-Mg anodes in deep Sw have reported reduced efficiency, due to rapid passivation at higher pressures.

The present work showed that Al alloy's performance remained stable even under varying Sw conductivities, suggesting better long-term corrosion resistance. This finding aligns with the improved anodic behaviour of Al alloys in highly saline environments, as indicated by [26]. These comparisons highlight the enhanced electrochemical characteristics of the as-fabricated Al alloy anodes, suggesting their suitability for more challenging marine environments compared to previously used SA.

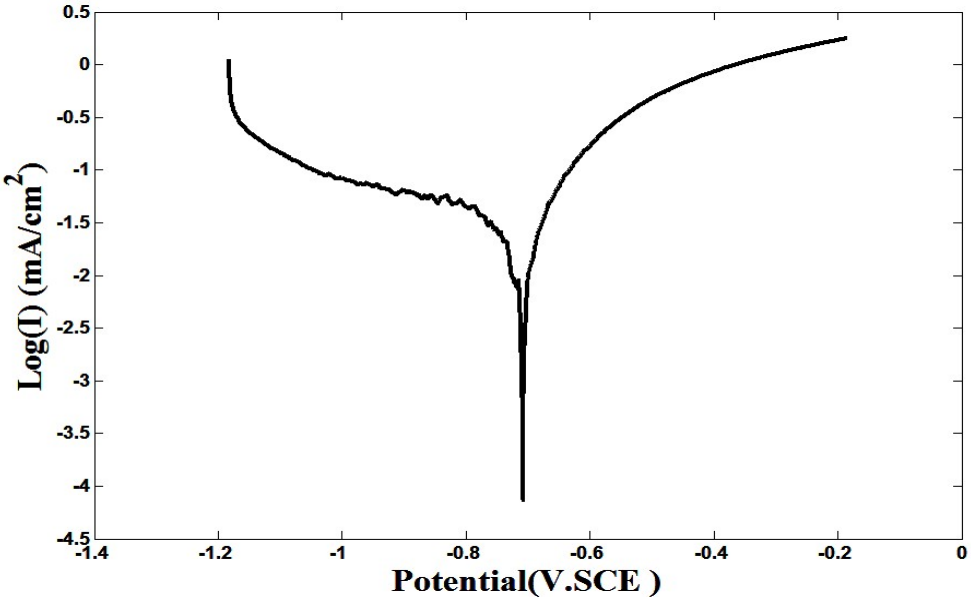

Figure 10: PDP curve recorded for the steel cathode.

Contour plots depicting E and j from CP on the steel cathode, considering a Sw conductivity of 2.16 S/m and DAC of 1 mm, are illustrated in Fig. 11. E from CP ranged from -0.9286 *vs.* SCE to -0.7079 *vs.* SCE. Notably, E in the area facing the anode was the lowest, at -0.93286 *vs.* SCE, and it increased with the distance away from the anode. Examining the distribution of j from CP, the contour clearly illustrates that the highest value of 13.543 mA/cm² was seen in the area facing the anode, diminishing as the distance from the anode increased.

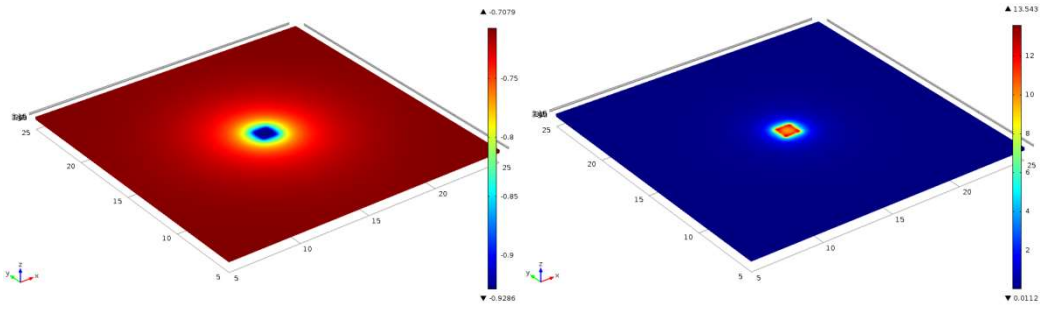

(a) **(b)**

Figure 11: Contour plot of illustrating **(a)** E and **(b)** j from CP.

To demonstrate the impact of varying DAC and adjusting Sw conductivity on the attenuation of E and j from CP, DAC was systematically varied from 0.5 to 2 cm, and Sw conductivity from 2 to 5 S/m. Contour plots showcasing E and j from CP on the steel cathode, with varying DAC and Sw conductivity, are depicted in Figs. 12-15, respectively.

Protection potentials for steel in Sw recommended by [27, 28] with respect to various reference electrodes, are as follows: 800 mV/Ag-AgCl, -780 mV/SCE, -530 mV/standard hydrogen electrode and -850 mV/$CuSO_4$. To define the distance protected by the anode, the anode's operational range was considered.

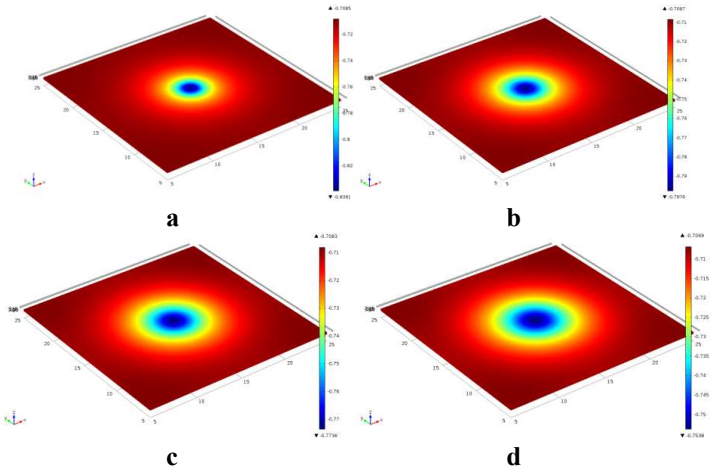

Figure 12: Contour plot illustrating E from CP along the steel cathode, at different DAC- **(a)** 0.5 cm, **(b)** 1 cm, **(c)** 1.5 cm and **(d)** 2 cm.

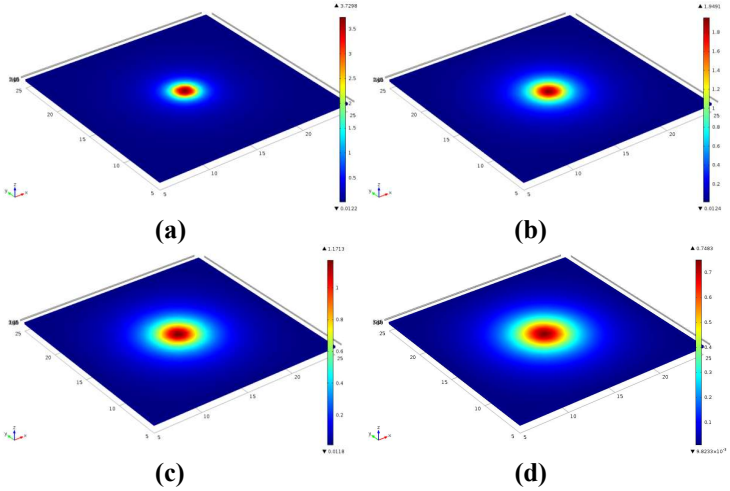

Figure 13: Contour plot representing j along the steel cathode, at various DAC -**(a)** 0.5, **(b)** 1, **(c)** 1.5 and **(d)** 2 cm.

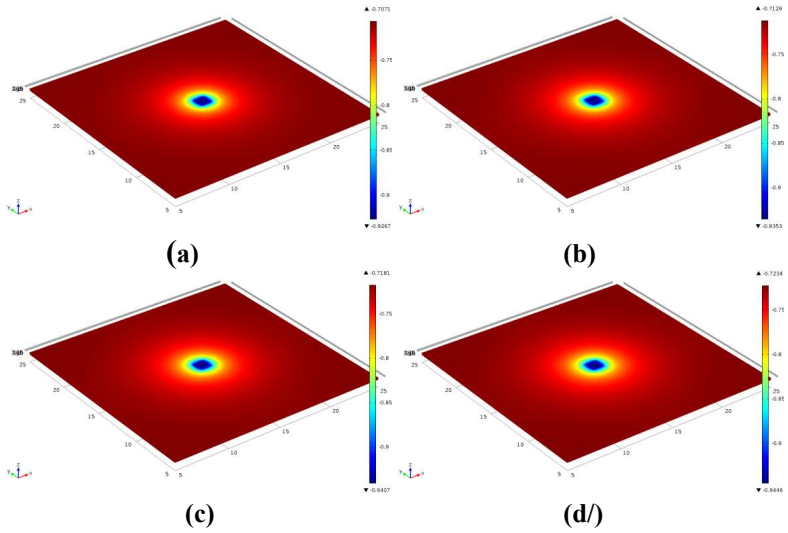

Figure 14: Contour plot demonstrating E from CP along the steel cathode with varying Sw conductivity-**(a)** 2 s/m, **(b)** 3 s/m, **(c)** 4 s/m, **(d)** 5 s/m.

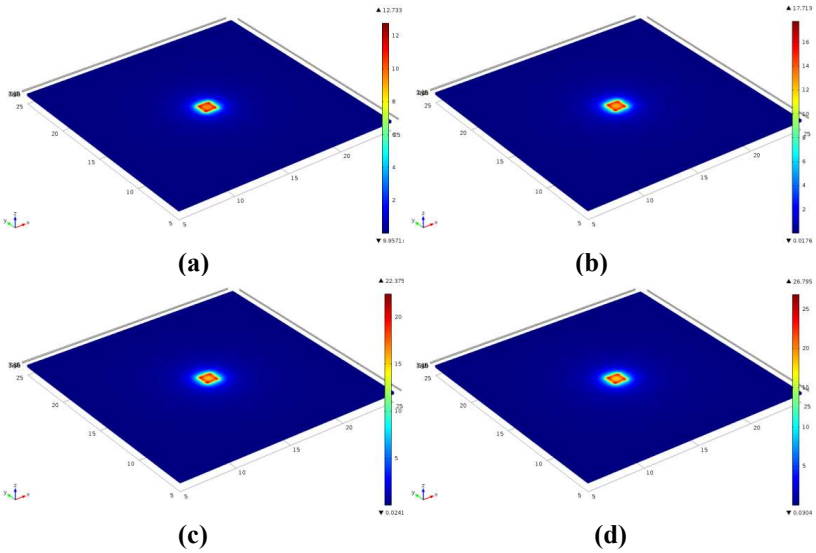

Figure 15: Contour plot representing CP j along the steel cathode with varying Sw conductivity **(a)** 2 s/m, **(b)** 3 s/m, **(c)** 4 s/m, **(d)** 5 s/m.

Figs. 16 and 17 depict, respectively, the attenuation of protection E and j with varying Sw conductivity and different DAC. In Fig. 16, the anode's operational range is at its peak, reaching 1.42 cm for a DAC of 5 mm and diminishing with an increase in it. For DAC values of 15 and 20 mm, the steel cathode remained unprotected from corrosion, with the operational range of 0 cm.

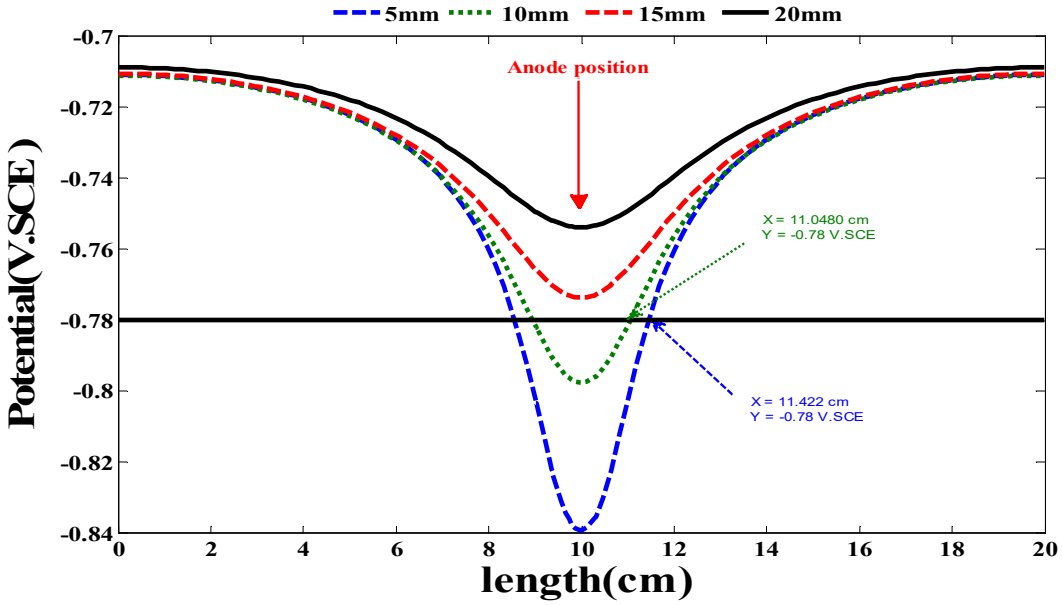

Figure 16: Attenuation of E from CP at various DAC.

In Fig. 17, the operational range of the anode achieved its maximum value at 2.03 cm, for a Sw conductivity of 5 S/m, and decreased with decreasing Sw conductivity: 1.86, 1.68 and 1.49 cm, for 4, 3 and 2 S/m, respectively. Table 6 provides a comprehensive overview of the areas protected by Al alloy anode, considering Sw conductivity ranging from 2 to 5 S/m, and DAC from 5 to 20 mm.

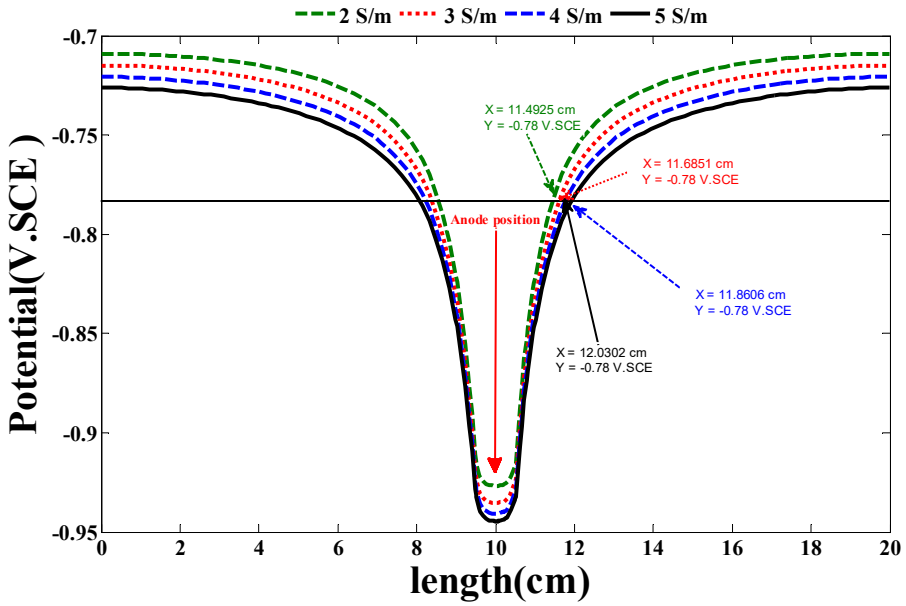

Figure 17: Attenuation of E from CP with varying Sw conductivity.

Table 6: Areas protected by Al alloy anode.

Surface (cm^2)		Sw conductivity (S/m)			
		2	3	4	5
DAC (mm)	5	6.154	8.445	10.74	13.196
	10	3.140	5.554	8.038	10.746
	15	0	0.283	2.834	5.722
	20	0	0	0	0

As per the results, an increase in conductivity expanded the area protected by the anode. Conversely, a decrease in DAC diminished the protected area. Notably, when D.A.C was 20 mm, the steel cathode remained unprotected from corrosion. The highest protected area by the anode, at 13.196 cm^2, was seen when the conductivity was 5 S/m and DAC was 5 mm. For effective CP, DAC should not exceed 0.5 mm.

Conclusions

A thorough examination of electrochemical dissolution processes of pure Al and Al alloy, both employed as anodes for CP of steel structures in a Sw environment, was conducted in this study. The effectiveness of Al alloy anodes was simulated under various operational conditions that included diverse Sw conductivity levels and several DAC, employing FEM. The results revealed a significant activation of Al alloy relative to pure Al, as indicated by the shift in OCP values towards a more anodic direction, and an increase in j_{corr}. Simulation outcomes further highlighted the steel cathode's potential, which had a positive shift with an increasing DAC, and a negative shift with rising conductivity. Additionally, the protection j of the steel cathode decreased with an increase in DAC and increased with higher conductivity. Under specific conditions, such as a Sw conductivity of 5 S/m and DAC of 5 mm, the area protected by the anode reached its maximum value at

36,726 cm². Conversely, under conditions of Sw conductivity of 2 S/m and a DAC of 20 mm, the steel cathode remained vulnerable to corrosion.

Key conclusions derived from this investigation encompass: experimental findings indicate that Zn enhanced the surface activation of Al alloy by accelerating the kinetic dissolution process and inducing a more uniform attack morphology. In Al alloy corrosion process, alloying elements acted as corrosion centers, fostering activation through pitting propagation, thereby increasing the electrode's active area. The elimination of the current plateau in the anodic branch of pure Al polarization curve improved Al alloy anode's surface activity, resulting in more uniform dissolution. E from the steel cathode shifted positively with an increasing DAC and negatively with a rise in Sw conductivity. The protection j of the steel cathode decreased with an increase in DAC and increased with a rise in Sw conductivity. The area protected by the anode increased with the rise in Sw conductivity and decreased with higher DAC. Ensuring effective CP requires that DAC is kept within the critical threshold of 0.5 mm.

Data availability statement

All data related to this study is available within the manuscript

Funding

The authors assert that no financial support, grants, or other forms of assistance were obtained during the preparation of this manuscript.

Conflict of interest

The authors declare the absence of any pertinent financial or non-financial interests that could potentially influence the content disclosed in this manuscript.

Authors' contributions

M'hamed Ouadah: conceptualization; investigation; project administration; supervision; validation; writing, review and editing. **Abderrahmane Younes**: investigation; methodology; validation; writing original draft.

Abbreviations

Atm: atmosphere
CP: cathodic protection
$CuSO_4$: copper sulphate
DAC: distance between anode and cathode
E: potential
EIS: electrochemical impedance spectroscopy
E_{corr}: corrosion potential
FEM: finite element method
HCl: hydrochloric acid
HF: hydrofluoric acid
HNO_3: nitric acid
j: current density

j_{corr}: corrosion current density
OCP: open circuit potential
NaCl: sodium chloride
PDP: potentiodynamic polarization
R_{ct}: charge transfer resistance
R_p: polarization resistance
SA: sacrificial anode
SCE: saturated calomel electrode
SiC: silicon carbide
Sw: seawater

References

1. Li C, Hou CC, Chen L et al. Rechargeable Al-ion batteries. EnergyChem. 2021;3(2):100049. https://doi.org/10.1016/j.enchem.2020.100049
2. Das S, Manna SS, Pathak B. Recent trends in electrode and electrolyte design for aluminum batteries. ACS Omega. 2020;6:1043-1053. https://doi.org/10.1021/acsomega.0c04163
3. Sfameni S, Truant F, Visco A et al. Design and Development of Sustainable Nanotechnological Protective Systems in Surface Treatment. Diss University of Messina. 2022. https://hdl.handle.net/11570/3243553
4. Shibli SMA, Dilimon VS, Mohan A. Development of nickel incorporated aluminium alloy matrix as an efficient sacrificial anode. J Appl Electrochem. 2007;37:1015-1019. https://doi.org/10.1007/s10800-007-9342-0
5. Lameche-DS, Benchettara A, Kellou F et al. Electrochemical Behaviour of Pure Aluminium and Al–5 %Zn Alloy in 3 % NaCl Solution. Arab J Sci Eng. 2014;39:113-122. https://doi.org/10.1007/s13369-013-0876-7
6. Rein J, Zacate SBK, Mao and Lin S. A tutorial on asymmetric electrocatalysis. Chem Soc Rev. 2023;52:8106-8125. https://doi.org/10.1039/D3CS00511A
7. H Ferkous, A Dilemi, A Abdennouri, et al. Study of the electrochemical behavior of Al-Zn-In based sacrificial anodes in sea water. Rev Sci Technol Synth. 2023;29(1):36-43. eISSN: 2352-9717
8. Narwal N, Katyal D, Kataria N et al. Emerging micropollutants in aquatic ecosystems and nanotechnology-based removal alternatives: a review, Chemosphere. 2023;341:139945. https://doi.org/10.1016/j.chemosphere.2023.139945
9. Shibli SMA, Gireesh VS. Activation of aluminium alloy sacrificial anodes by selenium. Corros Sci. 2005;47(8):2091-2097. https://doi.org/10.1016/j.corsci.2004.09.010
10. Olubunmi AT, Hannah AO, Ekwueme C et al. Cathodic Protection of Stainless and Galvanised Steels in Marine Environments Using Aluminium and Zinc as Sacrificial Anodes. Environments. 2024;11(4. ISSN: 2458-9403
11. Xiong W, Xiong W, Qi G T et al. Anodic dissolution of Al sacrificial anode in NaCl solution containing Ce. Corros Sci. 2011;53(4):1298-1303. https://doi.org/101016/jcorsci201101001

12. Alvira D, Antorán D, Manyà JJ. Assembly and electrochemical testing of renewable carbon-based anodes in SIBs: A practical guide. J Ener Chem. 2022;75:457-477. https://doi.org/0.1016/j.jechem.2022.09.002
13. Rath J, Ramasubramanian B, Ramakrishna S et al. Advancements in metalloid anodes (Si/Ge/B) for air batteries. Mem-Mat Dev Circ Syst. 2024;7:100097. https://doi.org/10.1016/j.memori.2023.100097
14. Blanc LE, Kundu D, Nazar LF. Scientific challenges for the implementation of Zn-ion batteries. Joule. 2020;4(4):771-799. https://doi.org/10.1016/j.joule.2020.03.002
15. Sun H, Liu L, Li Y et al. The performance of Al–Zn–In–Mg–Ti sacrificial anode in simulated deep water environment. Corros Sci. 2013;77:77-87. https://doi.org/10.1016/j.corsci.2013.07.029
16. Fischer KP. Anode Performance Data at High Pressure and Temperature: A Laboratory Study in Natural Seawater. Corrosion. 91/235, NACE, Houston, TX. Per Copy$ 5 (1991).
17. Ouadah M, Touhami O, Ibtiouen R et al. Method for Diagnosis of the Effect of AC on the X70 Pipeline due to an Inductive Coupling Caused by HVPL. IET Sci Measur Technol. 2017;11(6):766-772. https://doi.org/10.1049/iet-smt.2016.0519
18. Zhang P, Liu X, Xue J et al. The role of microstructural evolution in improving energy conversion of Al-based anodes for metal-air batteries. J Pow Sour. 2020;451:227806. https://doi.org/10.1016/j.jpowsour.2020.227806
19. Lameche-Djeghaba S, Benchettara A, Kellou F et al. Electrochemical behaviour of pure aluminium and Al–5% Zn alloy in 3% NaCl solution. Arab J Sci Eng. 2014;39:113-122. https://doi.org/10.1007/s13369-013-0876-7
20. Ma J, Wen J. Corrosion analysis of Al–Zn–In–Mg–Ti–Mn sacrificial anode alloy. J Allo Compo. 2010;496:110-115. https://doi.org/10.1016/j.jallcom.2010.02.174
21. Vignesh RV, Sathiya P. Sacrificial anode materials to protect marine grade steel structures: a review. Corros Rev. 2024;42(3):303-330. https://doi.org/10.1515/corrrev-2023-0099
22. Liang Y, Du Y, Zhu Z et al. Investigation on AC corrosion of aluminum alloy sacrificial anode in the artificial simulated seawater environment. Electrochim Acta. 2023;446:142002. https://doi.org/10.1016/j.electacta.2023.142002
23. Farooq A, Hamza M, Ahmed Q et al. Evaluating the performance of zinc and aluminum sacrificial anodes in artificial seawater. Electrochim Acta. 2019;314:135-141. https://doi.org/10.1016/j.electacta.2019.05.067
24. Flamini D, Saidman SB, Bessone BS et al. Aluminium activation produced by gallium. Corros Sci. 2006;48:1413-1425. https://doi.org/10.1016/j.corsci.2005.05.014
25. Wang H, Du, M Liang H et al. Study on Al-Zn-In Alloy as Sacrificial Anodes in Seawater Environment. J Ocean Univ Chin. 2019;18:889-895. https://doi.org/10.1007/s11802-019-3788-7

26. Fabris R, Masi G, Bignozzi MC. Corrosion Behavior of Aluminum Alloys in Different Alkaline Environments: Effect of Alloying Elements and Anodization Treatments. Coatings. 2024;14(2):240. https://doi.org/10.3390/coatings14020240
27. Diler E, Larché N, Thierry D. Carbon steel and Stainless-steel cathodic protection design data in Deep sea water–Influence of the environment on the biofilm cathodic activity. Inter Corros Conf Se. 2019, Nashville, USA, Article number 13124.
28. Halil MA, Ahmied EK. Steel Corrosion Control in Seawater Using Zinc sacrificial anode. Seb Univ J Pure Appl Sci. 2019;18(2). https://doi.org/10.51984/jopas.v18i2.335